

Augmenting Density Matrix Renormalization Group with Disentglers

Xiangjian Qian¹ and Mingpu Qin^{1,*}

¹*Key Laboratory of Artificial Structures and Quantum Control (Ministry of Education),
School of Physics and Astronomy, Shanghai Jiao Tong University, Shanghai 200240, China*

(Dated: April 13, 2023)

Density Matrix Renormalization Group (DMRG) and its extensions in the form of Matrix Product States (MPS) are arguably the choice for the study of one dimensional quantum systems in the last three decades. However, due to the limited entanglement encoded in the wave-function ansatz, to maintain the accuracy of DMRG with the increase of the system size in the study of two dimensional systems, exponentially increased resources are required, which limits the applicability of DMRG to only narrow systems. In this work, we introduce a new ansatz in which DMRG is augmented with disentanglers to encode area-law-like entanglement entropy (entanglement entropy supported in the new ansatz scales as l for a $l \times l$ system). In the new method, the $O(D^3)$ low computational cost of DMRG is kept (with an overhead of $O(d^4)$ and d the dimension of the physical degree of freedom). We perform benchmark calculations with this approach on the two dimensional transverse Ising and Heisenberg models. This new ansatz extends the power of DMRG in the study of two-dimensional quantum systems.

PACS numbers: 71.27.+a

The study of exotic phases and the phase transitions between them in strongly correlated quantum many-body systems is one of the largest challenges in condensed matter physics [1–3]. The main difficulty stems from the exponential growth of the Hilbert space dimension with the system size, which means brutal force approach can only handle very small systems. Analytic solution to quantum many-body systems is very rare [4–8]. So most studies of these systems rely on different types of numerical methods nowadays [9–17].

Density Matrix Renormalization Group (DMRG) [12–15, 18] is the most successful numerical methods for the study of one dimensional (1D) quantum many-body systems [19, 20] in the past decades. But it is known that the physics in two dimension (2D) is richer [21–30]. The direct application of DMRG to 2D systems is not as successful as the study of 1D cases. It was found that the required resource needs to increase exponentially with the system size in 2D if we want to maintain the accuracy [31].

It was realized later that the wave-functions obtained by DMRG are actually Matrix Product States (MPS) [32]. and the success of DMRG lies in the fact that the entanglement encoded in the wave-function satisfies the entropic area law [33–36] of 1D quantum systems. But MPS fail to capture the entropic area law for 2D systems which has to be remedied by exponentially large bond dimensions. To overcome this difficulty, MPS were generalized to high dimension in the perspective of Tensor Network States (TNS) [37, 38]. There is also effort to modify the MPS ansatz for 2D systems [39]. In TNS, the wave-function of a quantum many-body system is represented as the contraction of connected tensors with poly-

nomial parameters in contrast to the exponentially large Hilbert space. Different types of TNS were proposed in the past, like Projected Entangled Pair States (PEPS) [17, 40–44], Tree Tensor Network (TTN) [45–48], Multiscale Entanglement Renormalization ansatz (MERA) [49–52], and projected entangled simplex states (PESS) [53]. It can be easily proven that 2D PEPS, MERA, and PESS can capture the entropic area law for 2D quantum systems [36, 53, 54] which makes them better wave-function ansatz for 2D systems. Progress in the understanding of exotic states in 2D has been made with these TNS-related methods in the past [40, 55–59], but the high computational complexity hampers the wide application of them in the study of 2D systems. The typical cost of PEPS is $O(D^{10})$ [60] where D is the bond dimension (we notice that many attempts have been made to low the computation cost of PEPS [40, 61–63]) and $O(D^{16})$ [51] for MERA, which makes the calculation with large bond dimension infeasible and limit the power of these methods. For practical reason, because DMRG and MPS-based approaches are easy to be optimized and the computational cost is low, they are still widely used in the study of 2D (ladder or cylindrical) systems [64–69] by pushing the bond dimension to very large numbers, even though they cannot capture the entropic area law for 2D systems intrinsically.

In this work, we introduce a new MPS or DMRG based ansatz dubbed as Fully-augmented Matrix Product State (FAMPS) by generalizing the idea from augmented-TTN (aTTN) [45] and fully augmented-TTN (FATTN) [46] to MPS. The entanglement entropy encoded in both TTN and MPS are bounded by $\log(D)$, but MPS has a lower cost than TTN. In FAMPS, MPS is augmented with disentanglers to increase the entanglement encoded in the wave-function. In the simplest scheme, where disentanglers are placed directly in the physical layer and span only two sites, it can be proved that the entanglement

*qinmingpu@sjtu.edu.cn

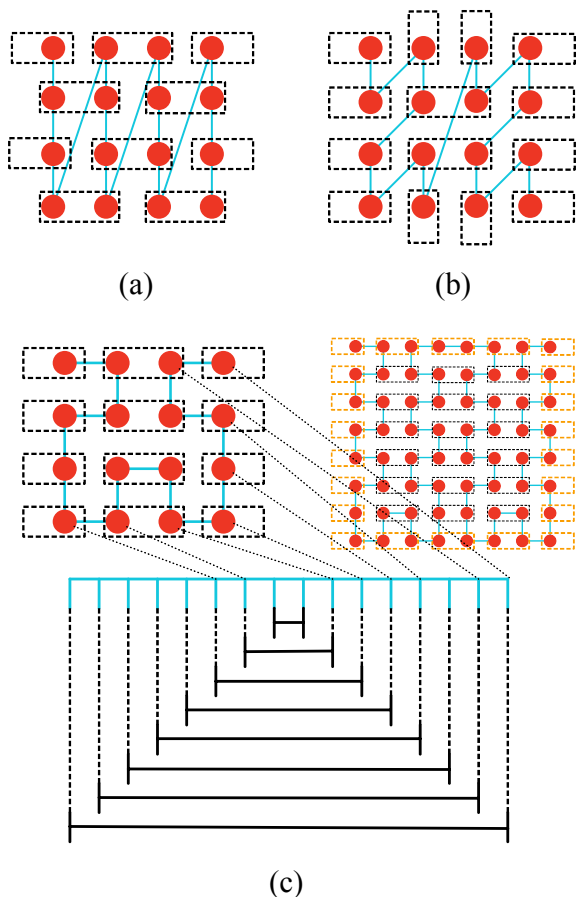


FIG. 1: Different schemes to arrange a 2D lattice into a 1D one in DMRG for periodic boundary conditions (PBC). The disentanglers in corresponding FAMPS are denoted as dashed rectangles. (a) The commonly adopted scheme for a 4×4 lattice. (b) A tree-type scheme for a 4×4 lattice (more details can be found in [46]). (c) A new scheme used in this work for 4×4 and 8×8 lattices and the corresponding one dimensional representation of the 4×4 lattice where the dashed black lines indicate how disentanglers act on MPS. The disentanglers at the edges denoted as dashed orange rectangles need to be rearranged for different boundary conditions. When augmented with disentanglers, the FAMPS encodes more entanglement in (b) and (c) than that in (a). See the main text for more discussion.

entropy captured in FAMPS scales as $l \ln(d^2)$ with l the measure of the cut with which the system is divided into two parts and d is the dimension of local Hilbert space. Most importantly, the low, i.e., $O(D^3)$ computational cost in DMRG is maintained in FAMPS.

Fully-Augmented Matrix Product States – An MPS is defined as

$$|\text{MPS}\rangle = \sum_{\{\sigma_i\}} \text{Tr}[A^{\sigma_1} A^{\sigma_2} A^{\sigma_3} \cdots A^{\sigma_n}] |\sigma_1 \sigma_2 \sigma_3 \cdots \sigma_n\rangle \quad (1)$$

where A is a rank-3 tensor with one physical index σ_i (with dimension d) and two auxiliary indices (with di-

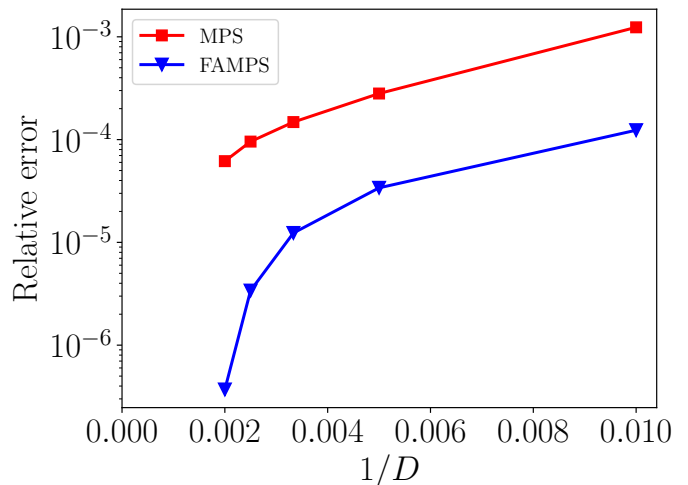


FIG. 2: Relative error of the ground state energy for FAMPS and MPS of the transverse Ising model near the critical point ($\lambda = 3.05$) for a 8×8 lattice with PBC. The scheme in Fig. 1 (c) is used. The reference energy is the Quantum Monte Carlo (QMC) result calculated by the stochastic series expansion (SSE) method with inverse temperature $\beta = 240$ [70, 71], which is $-3.24163(1)$. Since our best energy of FAMPS -3.2416288 (with $D = 500$) agrees with the reference energy within the error bar, the value of last point of FAMPS may be underestimated. We can find that the improvement of FAMPS over MPS is about one order of magnitude.

mension D).

Disentanglers are unitary matrices which transform the physical degrees of freedom of two sites. They are common building blocks in TNS which can reduce the local entanglement in the studied system [50, 72]. Following the strategy in [45, 46], we can place an additional disentangler layer on the physical layer of MPS to increase the entanglement in the wave-function as

$$|\text{FAMPS}\rangle = D(u)|\text{MPS}\rangle \quad (2)$$

where $D(u) = \prod_m u_m$ denotes the disentangler layer. Fig. 1 (c) shows the diagrammatic representation of FAMPS, where we can find that FAMPS is a more entangled wave-function than MPS [73].

As discussed in Ref. [46], there are two criteria or constraints when placing disentanglers. The first one is that there should be no two disentanglers sharing the same physical site. The other one is to place more disentanglers in places where the entanglement the ansatz wave-function can host is small. The first criterion ensures a comparable computational complexity with its predecessor (with a factor of d^4 at the worst case) The second criterion is to make the entanglement distribute as uniform as possible in the whole system. More specifically, we want to ensure the least entanglement in the wave-function for all different cuts as large as possible.

The special structure of FAMPS suggests that the optimization process of FAMPS can be divided into two steps. First, the disentanglers can be optimized using the

standard Evenly-Vidal algorithm [74]. Second, the rest of the tensors can be directly optimized with the traditional MPS or DMRG optimization procedure by solving eigenvalue problems [12]. The optimization of disentanglers and MPS tensors are performed alternatively for many times until the energy is converged. The details can be found in the supplementary materials. As discussed in the supplementary materials, the $O(D^3)$ cost of DMRG is kept in FAMPS with an additional factor of d^4 .

The arrangement of a 2D lattice to a 1D one in DMRG was extensively studied in the past [48, 75]. In the DMRG calculation, different arrangements have small effect on the accuracy as will be shown later. However, the way a 2D lattice is arranged in a 1D one is crucial when augmenting MPS with disentanglers, which determines the amount of entanglement the wave-function can encode. In Fig. 1, we show three different ways to arrange the 2D lattice in a 1D one. The scheme in Fig. 1 (a) is the most common used one in the literature. In this scheme, the entanglement is large if we cut the system horizontally, while only one bond is crossed if the system is cut vertically. This means an MPS in the scheme of Fig. 1 (a) can only encode an entanglement entropy $S \leq \ln(D)$. To augment MPS with disentanglers based on the scheme in Fig. 1 (a), we need to place all the disentanglers (the dashed rectangles in Fig. 1 (a)) horizontally according to the two criteria mentioned above. Because we can only place $L/2$ disentanglers horizontally in each column and the entanglement entropy contributed by each disentangler is maximally $\ln(d^2)$, the maximum entanglement entropy the FAMPS in Fig. 1 (a) can encode scales as $L \ln(d)$.

We have more efficient way to place the disentanglers. In Fig. 1 (c), we introduce another scheme to arrange the 2D lattice in a 1D one. The entanglement in the MPS in Fig. 1 (c) is more uniformly distributed than that in Fig. 1 (a) [76]. When augmented with disentanglers, the maximum entanglement entropy encoded in the FAMPS in Fig. 1 (c) is $L \ln(d^2)$ which is twice that in Fig. 1 (a) and in the aTTN [45]. Comparing to Fig. 1 (a), the number of crossed bonds with horizontal cut is reduced by a half, but even a small $D = d^4$ can support the $L \ln(d^2)$ entanglement entropy for these cuts. Actually Fig. 1 (c) is not the only scheme to support the $L \ln(d^2)$ entanglement entropy, another example is shown Fig. 1 (b), which is analyzed in Ref. [46] based on TTN. By placing the disentanglers appropriately, the arrangement following the Hilbert curve [48] can also support the $L \ln(d^2)$ entanglement entropy. In this work, we mainly focus on the scheme in Fig. 1 (c).

Results on the transverse Ising model – We first test FAMPS in the two dimensional transverse Ising model. The Hamiltonian of transverse Ising model is

$$H_{\text{Ising}} = - \sum_{\langle i,j \rangle} \sigma_i^z \sigma_j^z - \lambda \sum_i \sigma_i^x \quad (3)$$

where $\{\sigma_i^x, \sigma_i^z\}$ are Pauli matrices. In Fig. 2, we show the

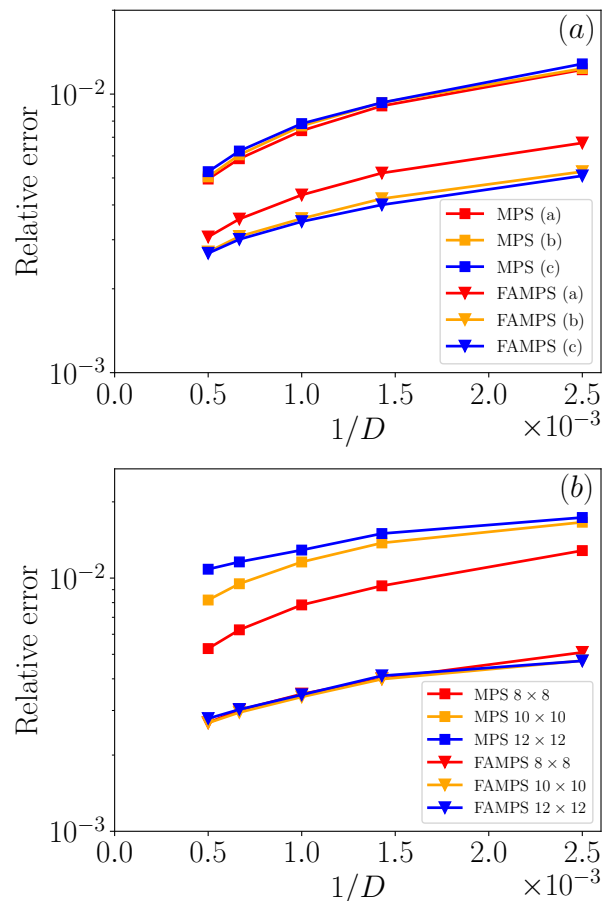


FIG. 3: Relative error of the ground state energy for FAMPS and MPS of the Heisenberg model with PBC. The reference energies are the numerically exact Quantum Monte Carlo results [10]. (a) We compare the results of different schemes in Fig. 1. ((a), (b), and (c) in the legend denote the different schemes in Fig. 1 (a), (b), and (c) respectively). We can see that the different schemes have little differences in DMRG energy. But after augmented with disentanglers, the FAMPS in Fig. 1 (c) gives lower energy than that in Fig. 1 (a) as expected. (b) We compare the results of different lattice sizes using the scheme in Fig. 1 (c). We can see that FAMPS accuracy is maintained with the increase of lattice size while MPS accuracy becomes worse as anticipated.

relative error of ground state energy from FAMPS and MPS simulations with $\lambda = 3.05$ (close to the critical point of the model). The scheme in Fig. 1 (c) is used to map the 2D lattice into 1D. The system is with size 8×8 and with PBC. As shown in Fig. 2, we can find that FAMPS is about one order of magnitude more accurate than MPS, which is similar to the improvement of FATTN over TTN in Ref. [46].

Results on the Heisenberg model – We also test FAMPS on the 2D Heisenberg model whose ground state is more entangled than the transverse Ising model. The Hamil-

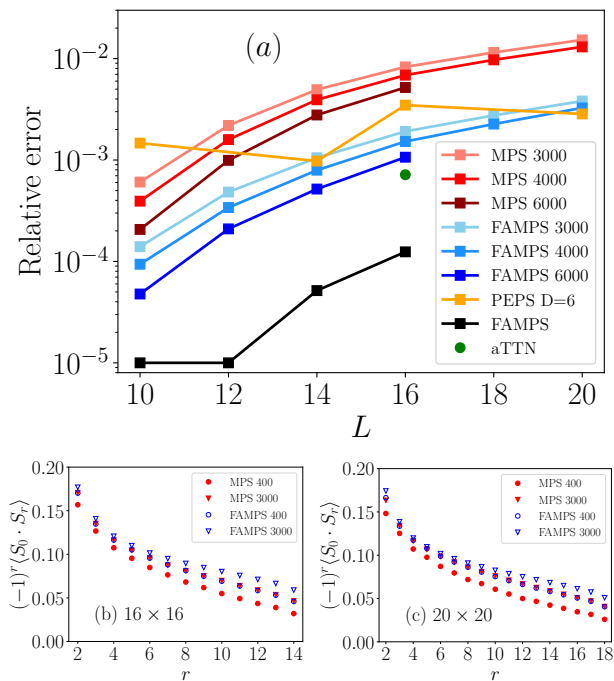


FIG. 4: (a) Relative error of the ground state energy for FAMPS, MPS, aTTN [45], and PEPS [60] of the Heisenberg model on square lattice with size from 10×10 to 20×20 (squares indicate open and periodic boundary conditions respectively). The reference energy is the numerically exact results obtained by Quantum Monte Carlo in [10, 40]. The black line is the extrapolated results for FAMPS at $D \rightarrow \infty$. For $L = 10$ and $L = 12$, because the extrapolated energies of FAMPS are exact within the error bar of Quantum Monte Carlo results, we set the relative errors of extrapolated FAMPS as 10^{-5} . From the plot, we can find FAMPS is able to outperform PEPS for $L \leq 20$. (b) and (c) show the corresponding spin correlations along the horizontal direction for 16×16 and 20×20 systems. FAMPS is able to give the same accuracy with a nearly one tenth bond dimension ($D = 400$) compared with MPS ($D = 3000$).

tonian of Heisenberg model is

$$H_{\text{Heisenberg}} = \sum_{\langle i,j \rangle} S_i \cdot S_j \quad (4)$$

where S_i denote the spin of site i . We consider only nearest neighboring interactions. Here, we take advantage of the $U(1)$ symmetry [77] in our simulation. We take the numerically exact Quantum Monte Carlo results [10, 40] as references. First, we calculate the ground state energy for 8×8 lattice with periodic boundary conditions to test FAMPS with different schemes to arrange the 2D lattice in 1D. Fig. 3 (a) shows the relative error of the ground state energy as a function of bond-dimension. We can find that the energies from MPS without disentangler layer have little differences for the three schemes in Fig. 1. This result agrees with the study in [48, 75] which show different arrangements can lead to increased numerical precision but not significant for 2D systems.

However, when augmented with disentanglers, FAMPS results in Fig. 3 (a) show the differences in accuracy is significant for different arrangement schemes. As expected, the FAMPS in Fig. 1 (c) is more accurate than that in Fig. 1 (a) because the entanglement encoded in the wave-function ansatz in (c) is larger. For the Heisenberg model, the improvement in accuracy is about half an order of magnitude.

We then test FAMPS with larger sizes using the scheme in Fig. 1 (c) In Fig. 3 (b), we show the relative error of the ground state energy for lattice sizes 8×8 , 10×10 , and 12×12 . The most important finding in these results is that the accuracy of FAMPS is maintained with the increase of lattice size, despite the accuracy of MPS decreases with the increase of lattice size as expected. This property makes FAMPS a promising method in the study of two dimensional systems in the future.

We also test FAMPS for Heisenberg model with open boundary conditions. We find that there exists a critical bond dimension after which the energies calculated by FAMPS and MPS are identical in the $U(1)$ symmetry imposed calculation (see the plot in the supplementary materials). This problem is caused by the absence of free parameters of disentanglers. The disentangler for spin $1/2$ degree of freedom ($d = 2$) has one free parameter under $U(1)$ symmetry and no free parameter under $SU(2)$ symmetry. When the bond dimension exceeds the critical value, the state in $U(1)$ symmetry imposed MPS calculation nearly restores the $SU(2)$ symmetry. Thus, the extra disentangler layer has no effect and FAMPS and MPS give the same results. The transverse Ising model has $Z(2)$ symmetry with two free parameters in the disentangler, which is the reason why there is no critical bond dimension in Fig. 2. The details of analyzing the number of free parameters in the disentanglers can be found in the Supplementary Materials.

To solve this problem, we block two sites into one to increase the number of free parameters of disentangler and impose $SU(2)$ symmetry in the calculation. Fig. 4 (a) shows the relative error of ground state energy calculated by MPS and FAMPS for different lattice sizes. We can find that the energies of FAMPS are lower than PEPS results with bond-dimension $D=6$ for $L \leq 20$ in Fig. 4 (a). When extrapolated to the infinite bond dimension limit for both FAMPS and aTTN, FAMPS is also more accurate than aTTN. Fig. 4 (b) and (c) show the corresponding spin correlations along the horizontal direction. FAMPS gives the same results as MPS with a nearly one tenth bond dimension for the correlation function.

At last, we show preliminary results of FAMPS on the more challenging J_1 - J_2 Heisenberg model. We focus on the most difficult point with $J_2/J_1 = 0.5$. The comparison of ground state energy for a 8×8 system with PBC is listed in Table. I. We can find that the FAMPS energy with $D = 12000$ is more accurate than previous DMRG energy with $D = 32000$ and FAMPS with $D = 24000$ gives the most accurate energy.

Conclusions – In this work, we propose a new

Method	Energy per site
CNN	-0.49639(2) [78]
RBM+PP	-0.498460(6) [79]
DMRG D=24000	-0.497961 [64]
DMRG D=32000	-0.498175 [64]
VMC	-0.49656(1) [80]
FAMPS D=12000 (this work)	-0.498184
FAMPS D=24000 (this work)	-0.498508

TABLE I: The comparison of the ground state energy of the J1-J2 Heisenberg model ($J_2/J_1 = 0.5$) on a 8×8 square lattice with periodic boundary conditions.

ansatz, FAMPS, by augmenting MPS with disentanglers. FAMPS can encode area-law-like entanglement entropy for two dimensional quantum systems and at the same time keeps the low $O(D^3)$ computational cost (with an overhead of $O(d^4)$). We carry out benchmark calculations of FAMPS on the 2D transverse Ising model near critical point and the 2D Heisenberg model. FAMPS pro-

vides a useful approach to extend the power of DMRG for the study of difficult 2D problems [64]. FAMPS can be generalized to encode more entanglement by placing multiple layers of disentanglers to MPS. The linearly scaled entanglement encoded in FAMPS can also benefit many other MPS based approaches, e.g., the simulation of time evolution or the dynamic properties [81–83]. FAMPS is also applicable to any other lattices by rearranging the studied system in a one dimension way.

Acknowledgments

The calculation in this work is carried out with Quimb [84] and TensorKit [85]. MQ acknowledges the support from the National Key Research and Development Program of MOST of China (2022YFA1405400), the National Natural Science Foundation of China (Grant No. 12274290) and the sponsorship from Yangyang Development Fund.

-
- [1] D. Cabra, A. Honecker, and P. Pujol, *Modern Theories of Many-Particle Systems in Condensed Matter Physics*, vol. 843 (2012), ISBN 978-3-642-10448-0.
- [2] X. G. Wen, *Quantum field theory of many-body systems: from the origin of sound to an origin of light and electrons* (Oxford University Press, Oxford, 2007), URL <https://cds.cern.ch/record/803748>.
- [3] E. C. Marino, *Quantum Field Theory Approach to Condensed Matter Physics* (Cambridge University Press, Cambridge, 2017).
- [4] A. J. Berlinsky and A. B. Harris, *The Ising Model: Exact Solutions* (Springer International Publishing, Cham, 2019), pp. 441–476, ISBN 978-3-030-28187-8, URL https://doi.org/10.1007/978-3-030-28187-8_17.
- [5] J. Dukelsky, S. Pittel, and G. Sierra, *Rev. Mod. Phys.* **76**, 643 (2004), URL <https://link.aps.org/doi/10.1103/RevModPhys.76.643>.
- [6] E. H. Lieb and F. Y. Wu, *Phys. Rev. Lett.* **20**, 1445 (1968), URL <https://link.aps.org/doi/10.1103/PhysRevLett.20.1445>.
- [7] Y. Qiao, P. Sun, Z. Xin, J. Cao, and W.-L. Yang, *Journal of Physics A: Mathematical and Theoretical* **53**, 075205 (2020), URL <https://doi.org/10.1088/1751-8121/ab6a32>.
- [8] H. Zou, E. Zhao, X.-W. Guan, and W. V. Liu, *Phys. Rev. Lett.* **122**, 180401 (2019), URL <https://link.aps.org/doi/10.1103/PhysRevLett.122.180401>.
- [9] J. E. Hirsch, R. L. Sugar, D. J. Scalapino, and R. Blankenbecler, *Phys. Rev. B* **26**, 5033 (1982), URL <https://link.aps.org/doi/10.1103/PhysRevB.26.5033>.
- [10] A. W. Sandvik, *Phys. Rev. B* **56**, 11678 (1997), URL <https://link.aps.org/doi/10.1103/PhysRevB.56.11678>.
- [11] W. J. Huggins, B. A. O’Gorman, N. C. Rubin, D. R. Reichman, R. Babbush, and J. Lee, *Nature* **603**, 416 (2022), ISSN 1476-4687, URL <https://doi.org/10.1038/s41586-021-04351-z>.
- [12] S. R. White, *Phys. Rev. Lett.* **69**, 2863 (1992), URL <https://link.aps.org/doi/10.1103/PhysRevLett.69.2863>.
- [13] S. R. White, *Phys. Rev. B* **48**, 10345 (1993), URL <https://link.aps.org/doi/10.1103/PhysRevB.48.10345>.
- [14] U. Schollwöck, *Rev. Mod. Phys.* **77**, 259 (2005), URL <https://link.aps.org/doi/10.1103/RevModPhys.77.259>.
- [15] U. Schollwöck, *Annals of Physics* **326**, 96 (2011), ISSN 0003-4916, January 2011 Special Issue, URL <https://www.sciencedirect.com/science/article/pii/S0003491610001752>.
- [16] J. P. F. LeBlanc, A. E. Antipov, F. Becca, I. W. Bulik, G. K.-L. Chan, C.-M. Chung, Y. Deng, M. Ferrero, T. M. Henderson, C. A. Jiménez-Hoyos, et al. (Simons Collaboration on the Many-Electron Problem), *Phys. Rev. X* **5**, 041041 (2015), URL <https://link.aps.org/doi/10.1103/PhysRevX.5.041041>.
- [17] J. I. Cirac, D. Pérez-García, N. Schuch, and F. Verstraete, *Rev. Mod. Phys.* **93**, 045003 (2021), URL <https://link.aps.org/doi/10.1103/RevModPhys.93.045003>.
- [18] E. Stoudenmire and S. R. White, *Annual Review of Condensed Matter Physics* **3**, 111 (2012), <https://doi.org/10.1146/annurev-conmatphys-020911-125018>, URL <https://doi.org/10.1146/annurev-conmatphys-020911-125018>.
- [19] E. M. Stoudenmire, L. O. Wagner, S. R. White, and K. Burke, *Phys. Rev. Lett.* **109**, 056402 (2012), URL <https://link.aps.org/doi/10.1103/PhysRevLett.109.056402>.
- [20] K. Hida, *Phys. Rev. Lett.* **83**, 3297 (1999), URL <https://link.aps.org/doi/10.1103/PhysRevLett.83.3297>.
- [21] H. Nakano, Y. Minami, and S.-i. Sasa, *Phys. Rev. Lett.* **126**, 160604 (2021), URL <https://link.aps.org/doi/10.1103/PhysRevLett.126.160604>.

- 10.1103/PhysRevLett.126.160604.
- [22] I. A. Verzhbitskiy, D. Voiry, M. Chhowalla, and G. Eda, *2D Materials* **7**, 035013 (2020), URL <https://doi.org/10.1088/2053-1583/ab8690>.
- [23] G. E. Astrakharchik, I. L. Kurbakov, D. V. Sychev, A. K. Fedorov, and Y. E. Lozovik, *Phys. Rev. B* **103**, L140101 (2021), URL <https://link.aps.org/doi/10.1103/PhysRevB.103.L140101>.
- [24] B. Dalla Piazza, M. Mourigal, N. B. Christensen, G. J. Nilsen, P. Tregenna-Piggott, T. G. Perring, M. Enderle, D. F. McMorrow, D. A. Ivanov, and H. M. Rønnow, *Nature Physics* **11**, 62 (2015), ISSN 1745-2481, URL <https://doi.org/10.1038/nphys3172>.
- [25] A. W. W. Ludwig, D. Poilblanc, S. Trebst, and M. Troyer, *New Journal of Physics* **13**, 045014 (2011), URL <https://doi.org/10.1088/1367-2630/13/4/045014>.
- [26] M. Brooks, M. Lemeshko, D. Lundholm, and E. Yakaboylu, *Phys. Rev. Lett.* **126**, 015301 (2021), URL <https://link.aps.org/doi/10.1103/PhysRevLett.126.015301>.
- [27] C. Han, Z. Iftikhar, Y. Kleorin, A. Anthore, F. Pierre, Y. Meir, A. K. Mitchell, and E. Sela, *Phys. Rev. Lett.* **128**, 146803 (2022), URL <https://link.aps.org/doi/10.1103/PhysRevLett.128.146803>.
- [28] D. Arovas, J. R. Schrieffer, and F. Wilczek, *Phys. Rev. Lett.* **53**, 722 (1984), URL <https://link.aps.org/doi/10.1103/PhysRevLett.53.722>.
- [29] B. I. Halperin, *Phys. Rev. Lett.* **52**, 1583 (1984), URL <https://link.aps.org/doi/10.1103/PhysRevLett.52.1583>.
- [30] F. Wilczek, *Phys. Rev. Lett.* **49**, 957 (1982), URL <https://link.aps.org/doi/10.1103/PhysRevLett.49.957>.
- [31] S. Liang and H. Pang, *Phys. Rev. B* **49**, 9214 (1994), URL <https://link.aps.org/doi/10.1103/PhysRevB.49.9214>.
- [32] S. Östlund and S. Rommer, *Phys. Rev. Lett.* **75**, 3537 (1995), URL <https://link.aps.org/doi/10.1103/PhysRevLett.75.3537>.
- [33] M. B. Plenio, J. Eisert, J. Dreißig, and M. Cramer, *Phys. Rev. Lett.* **94**, 060503 (2005), URL <https://link.aps.org/doi/10.1103/PhysRevLett.94.060503>.
- [34] G. Vidal, J. I. Latorre, E. Rico, and A. Kitaev, *Phys. Rev. Lett.* **90**, 227902 (2003), URL <https://link.aps.org/doi/10.1103/PhysRevLett.90.227902>.
- [35] M. Srednicki, *Phys. Rev. Lett.* **71**, 666 (1993), URL <https://link.aps.org/doi/10.1103/PhysRevLett.71.666>.
- [36] J. Eisert, M. Cramer, and M. B. Plenio, *Rev. Mod. Phys.* **82**, 277 (2010), URL <https://link.aps.org/doi/10.1103/RevModPhys.82.277>.
- [37] R. Orús, *Nature Reviews Physics* **1**, 538 (2019), ISSN 2522-5820, URL <https://doi.org/10.1038/s42254-019-0086-7>.
- [38] J. C. Bridgeman and C. T. Chubb, *Journal of Physics A: Mathematical and Theoretical* **50**, 223001 (2017), URL <https://doi.org/10.1088/1751-8121/aa6dc3>.
- [39] G. Lami, G. Carleo, and M. Collura, *Phys. Rev. B* **106**, L081111 (2022), URL <https://link.aps.org/doi/10.1103/PhysRevB.106.L081111>.
- [40] W.-Y. Liu, Y.-Z. Huang, S.-S. Gong, and Z.-C. Gu, *Phys. Rev. B* **103**, 235155 (2021), URL <https://link.aps.org/doi/10.1103/PhysRevB.103.235155>.
- [41] G. Scarpa, A. Molnár, Y. Ge, J. J. García-Ripoll, N. Schuch, D. Pérez-García, and S. Iblisdir, *Phys. Rev. Lett.* **125**, 210504 (2020), URL <https://link.aps.org/doi/10.1103/PhysRevLett.125.210504>.
- [42] H.-J. Liao, J.-G. Liu, L. Wang, and T. Xiang, *Phys. Rev. X* **9**, 031041 (2019), URL <https://link.aps.org/doi/10.1103/PhysRevX.9.031041>.
- [43] C. Hubig, *SciPost Phys.* **5**, 47 (2018), URL <https://scipost.org/10.21468/SciPostPhys.5.5.047>.
- [44] L. Vanderstraeten, L. Burgelman, B. Ponsioen, M. Van Damme, B. Vanhecke, P. Corboz, J. Haegeman, and F. Verstraete, *Phys. Rev. B* **105**, 195140 (2022), URL <https://link.aps.org/doi/10.1103/PhysRevB.105.195140>.
- [45] T. Felser, S. Notarnicola, and S. Montangero, *Phys. Rev. Lett.* **126**, 170603 (2021), URL <https://link.aps.org/doi/10.1103/PhysRevLett.126.170603>.
- [46] X. Qian and M. Qin, *Phys. Rev. B* **105**, 205102 (2022), URL <https://link.aps.org/doi/10.1103/PhysRevB.105.205102>.
- [47] P. Silvi, F. Tschirsich, M. Gerster, J. Jünemann, D. Jaschke, M. Rizzi, and S. Montangero, *SciPost Phys. Lect. Notes* p. 8 (2019), URL <https://scipost.org/10.21468/SciPostPhysLectNotes.8>.
- [48] G. Cataldi, A. Abedi, G. Magnifico, S. Notarnicola, N. D. Pozza, V. Giovannetti, and S. Montangero, *Quantum* **5**, 556 (2021), ISSN 2521-327X, URL <https://doi.org/10.22331/q-2021-09-29-556>.
- [49] J. C. Bridgeman, A. O'Brien, S. D. Bartlett, and A. C. Doherty, *Phys. Rev. B* **91**, 165129 (2015), URL <https://link.aps.org/doi/10.1103/PhysRevB.91.165129>.
- [50] G. Vidal, *Phys. Rev. Lett.* **101**, 110501 (2008), URL <https://link.aps.org/doi/10.1103/PhysRevLett.101.110501>.
- [51] G. Evenbly and G. Vidal, *Phys. Rev. Lett.* **102**, 180406 (2009), URL <https://link.aps.org/doi/10.1103/PhysRevLett.102.180406>.
- [52] G. Vidal, *Phys. Rev. Lett.* **99**, 220405 (2007), URL <https://link.aps.org/doi/10.1103/PhysRevLett.99.220405>.
- [53] Z. Y. Xie, J. Chen, J. F. Yu, X. Kong, B. Normand, and T. Xiang, *Phys. Rev. X* **4**, 011025 (2014), URL <https://link.aps.org/doi/10.1103/PhysRevX.4.011025>.
- [54] F. Verstraete, M. M. Wolf, D. Perez-Garcia, and J. I. Cirac, *Phys. Rev. Lett.* **96**, 220601 (2006), URL <https://link.aps.org/doi/10.1103/PhysRevLett.96.220601>.
- [55] G. Evenbly and G. Vidal, *Phys. Rev. Lett.* **104**, 187203 (2010), URL <https://link.aps.org/doi/10.1103/PhysRevLett.104.187203>.
- [56] P. Corboz and F. Mila, *Phys. Rev. Lett.* **112**, 147203 (2014), URL <https://link.aps.org/doi/10.1103/PhysRevLett.112.147203>.
- [57] H. J. Liao, Z. Y. Xie, J. Chen, Z. Y. Liu, H. D. Xie, R. Z. Huang, B. Normand, and T. Xiang, *Phys. Rev. Lett.* **118**, 137202 (2017), URL <https://link.aps.org/doi/10.1103/PhysRevLett.118.137202>.
- [58] B.-X. Zheng, C.-M. Chung, P. Corboz, G. Ehlers, M.-P. Qin, R. M. Noack, H. Shi, S. R. White, S. Zhang, and G. K.-L. Chan, *Science* **358**, 1155 (2017), ISSN 0036-8075, 1095-9203, URL <http://science.sciencemag.org/content/358/6367/1155>.
- [59] W.-Y. Liu, S.-S. Gong, Y.-B. Li, D. Poilblanc, W.-Q. Chen, and Z.-C. Gu, *Science Bulletin* **67**, 1034 (2022), ISSN 2095-9273, URL <https://www.sciencedirect.com>.

- com/science/article/pii/S2095927322001001.
- [60] M. Lubasch, J. I. Cirac, and M.-C. Bañuls, *Phys. Rev. B* **90**, 064425 (2014), URL <https://link.aps.org/doi/10.1103/PhysRevB.90.064425>.
- [61] Z. Y. Xie, H. J. Liao, R. Z. Huang, H. D. Xie, J. Chen, Z. Y. Liu, and T. Xiang, *Phys. Rev. B* **96**, 045128 (2017), URL <https://link.aps.org/doi/10.1103/PhysRevB.96.045128>.
- [62] M. T. Fishman, L. Vanderstraeten, V. Zauner-Stauber, J. Haegeman, and F. Verstraete, *Phys. Rev. B* **98**, 235148 (2018), URL <https://link.aps.org/doi/10.1103/PhysRevB.98.235148>.
- [63] M. Qin, *Phys. Rev. B* **102**, 125143 (2020), URL <https://link.aps.org/doi/10.1103/PhysRevB.102.125143>.
- [64] S.-S. Gong, W. Zhu, D. N. Sheng, O. I. Motrunich, and M. P. A. Fisher, *Phys. Rev. Lett.* **113**, 027201 (2014), URL <https://link.aps.org/doi/10.1103/PhysRevLett.113.027201>.
- [65] S. Yan, D. A. Huse, and S. R. White, *Science* **332**, 1173 (2011), <https://www.science.org/doi/pdf/10.1126/science.1201080>, URL <https://www.science.org/doi/abs/10.1126/science.1201080>.
- [66] M. Qin, C.-M. Chung, H. Shi, E. Vitali, C. Hubig, U. Schollwöck, S. R. White, and S. Zhang (Simons Collaboration on the Many-Electron Problem), *Phys. Rev. X* **10**, 031016 (2020), URL <https://link.aps.org/doi/10.1103/PhysRevX.10.031016>.
- [67] H.-C. Jiang and S. A. Kivelson, *Phys. Rev. Lett.* **127**, 097002 (2021), URL <https://link.aps.org/doi/10.1103/PhysRevLett.127.097002>.
- [68] S. Gong, W. Zhu, and D. N. Sheng, *Phys. Rev. Lett.* **127**, 097003 (2021), URL <https://link.aps.org/doi/10.1103/PhysRevLett.127.097003>.
- [69] S. Jiang, D. J. Scalapino, and S. R. White, *Proceedings of the National Academy of Sciences* **118**, e2109978118 (2021), <https://www.pnas.org/doi/pdf/10.1073/pnas.2109978118>, URL <https://www.pnas.org/doi/abs/10.1073/pnas.2109978118>.
- [70] O. F. Syljuåsen and A. W. Sandvik, *Phys. Rev. E* **66**, 046701 (2002), URL <https://link.aps.org/doi/10.1103/PhysRevE.66.046701>.
- [71] The calculation of SSE QMC is performed with IsingMonteCarlo package at <https://github.com/Renmusxd/IsingMonteCarlo>.
- [72] S.-J. Ran, *Phys. Rev. A* **101**, 032310 (2020), URL <https://link.aps.org/doi/10.1103/PhysRevA.101.032310>.
- [73] By contracting the additional disentangler layer in Fig. 1 (c) into the original MPS wave-function, the effective bond dimension for the resulting MPS is much larger than the original MPS. Thus, FAMPS is a more entangled wave-function than MPS.
- [74] G. Evenbly and G. Vidal, *Phys. Rev. B* **79**, 144108 (2009), URL <https://link.aps.org/doi/10.1103/PhysRevB.79.144108>.
- [75] T. Xiang, J. Lou, and Z. Su, *Phys. Rev. B* **64**, 104414 (2001), URL <https://link.aps.org/doi/10.1103/PhysRevB.64.104414>.
- [76] We can still easily find vertical cut which crosses only one bond, but the number of these cuts is smaller.
- [77] S. Singh, R. N. C. Pfeifer, and G. Vidal, *Phys. Rev. B* **83**, 115125 (2011), URL <https://link.aps.org/doi/10.1103/PhysRevB.83.115125>.
- [78] K. Choo, T. Neupert, and G. Carleo, *Phys. Rev. B* **100**, 125124 (2019), URL <https://link.aps.org/doi/10.1103/PhysRevB.100.125124>.
- [79] Y. Nomura and M. Imada, *Phys. Rev. X* **11**, 031034 (2021), URL <https://link.aps.org/doi/10.1103/PhysRevX.11.031034>.
- [80] W.-J. Hu, F. Becca, A. Parola, and S. Sorella, *Phys. Rev. B* **88**, 060402 (2013), URL <https://link.aps.org/doi/10.1103/PhysRevB.88.060402>.
- [81] S. Paeckel, T. Köhler, A. Swoboda, S. R. Manmana, U. Schollwöck, and C. Hubig, *Annals of Physics* **411**, 167998 (2019), ISSN 0003-4916, URL <https://www.sciencedirect.com/science/article/pii/S0003491619302532>.
- [82] M. C. Bañuls, M. B. Hastings, F. Verstraete, and J. I. Cirac, *Phys. Rev. Lett.* **102**, 240603 (2009), URL <https://link.aps.org/doi/10.1103/PhysRevLett.102.240603>.
- [83] S. R. White and A. E. Feiguin, *Phys. Rev. Lett.* **93**, 076401 (2004), URL <https://link.aps.org/doi/10.1103/PhysRevLett.93.076401>.
- [84] J. Gray, *Journal of Open Source Software* **3**, 819 (2018).
- [85] The SU(2) symmetry code is developed with TensorKit package at <https://github.com/Jutho/TensorKit.jl>.

Supplementary Materials for “Augmenting Density Matrix Renormalization Group with Disentangler”

Xiangjian Qian¹ and Mingpu Qin^{1,*}

¹Key Laboratory of Artificial Structures and Quantum Control (Ministry of Education), School of Physics and Astronomy, Shanghai Jiao Tong University, Shanghai 200240, China

Optimization of FAMPS

We use a one dimensional representation of FAMPS (as shown in Fig. 1 (c) in the main text) to illustrate the optimization steps. The optimization process of FAMPS is similar as MPS which consists of the calculation of environment tensors and the solving of an eigenvalue problem. The difference is that in FAMPS the calculation of environment is more involved because of the disentangler layer. Here, we consider a Hamiltonian which only contains two-site operators,

$$H = \sum_{ij} h_{ij} \quad (1)$$

We first discuss the optimization of the tensors of MPS. Because disentanglers cannot share the same site, each term of H is mostly connected to two disentanglers. Thus, after the application of disentanglers, any two-site operator h_{ij} connects with at most four sites

$$h'_{ij} = D(u)^\dagger h_{ij} D(u) = u_{ik}^\dagger u_{jl}^\dagger h_{ij} u_{ik} u_{jl} = O_{ijkl} \quad (2)$$

where $D(u) = \prod_m u_m$ represents the disentangler layer. Other disentanglers not acting on sites i, j are annihilated due to $u^\dagger u = I$. The Hamiltonian H becomes

$$H' = D(u)^\dagger \sum_{ij} h_{ij} D(u) = \sum_{ij} h'_{ij} \quad (3)$$

where h'_{ij} is at most a four-site operator. So, a FAMPS with a Hamiltonian H is transformed to an MPS with an effective Hamiltonian H' . More specifically,

$$\begin{aligned} \langle \text{FAMPS} | H | \text{FAMPS} \rangle &= \langle \text{MPS} | D(u)^\dagger H D(u) | \text{MPS} \rangle \\ &= \langle \text{MPS} | H' | \text{MPS} \rangle \end{aligned} \quad (4)$$

Thus, we can follow the procedures in MPS to optimize MPS tensors in FAMPS. An environment of an MPS tensor for a four-site operator is shown in Fig. 1 (a). The contraction of it has a cost of $O(D^3)$. We need to calculate the environment for each term in the Hamiltonian H to get the overall environment.

For the optimization of disentanglers, we follow the procedure shown in Ref. [1, 2] where the key step is also the computation of environment. Here, after the application of disentanglers, any two-site operator h_{ij} is also at most a four-site operator

$$h''_{ij} = \prod_m u_m^\dagger h_{ij} \prod_{m \neq \{ik\}} u_m = u_{ik}^\dagger u_{jl}^\dagger h_{ij} u_{ik} u_{jl} = O'_{ijkl} \quad (5)$$

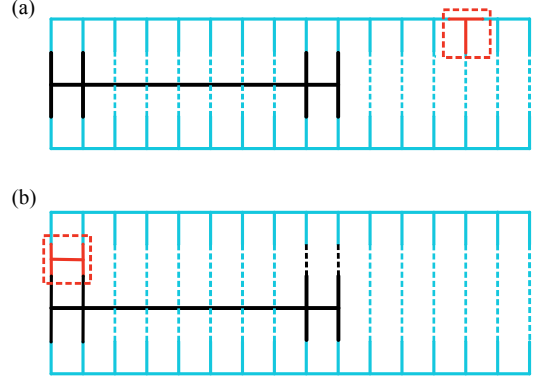


FIG. 1: (a) The environment for an MPS tensor. (b) The environment for a disentangler. The contractions of (a) and (b) can be performed with a computational cost of $O(D^3)$. The black line denotes a four-site operator. The red lines are the tensors to be optimized.

where u_{ik} is the disentangler we want to optimize. Fig. 1 (b) shows the corresponding environment for a disentangler, which can also be contracted with a complexity of $O(D^3)$. The overall environment only involves Hamiltonian terms which are directly attached to the disentangler u_{ik} , which makes the optimization of disentanglers very fast. All other Hamiltonian terms contribute a constant term to the energy expectation value and are independent of u_{ik} [1]. More specifically,

$$\begin{aligned} \langle \text{FAMPS} | H | \text{FAMPS} \rangle &= \langle \text{MPS} | D(u)^\dagger H D(u) | \text{MPS} \rangle \\ &= \langle \text{MPS} | \sum_p h''_p u_{ik} | \text{MPS} \rangle + C_{ik} \end{aligned} \quad (6)$$

where p represents the Hamiltonian terms that act on u_{ik} and $C_{ik} = \langle \text{MPS} | \sum_k h'_k | \text{MPS} \rangle$ with k the other Hamiltonian terms not acting on u_{ik} .

Overall, the optimization process of FAMPS is divided into two steps: the optimization of disentanglers and the optimization of the MPS tensors. For the optimization of disentanglers, the procedure is described as follows.

- (i) select a disentangler u , calculate the environments for this disentangler from the Hamiltonian terms that are directly attached to it, add them up to get the overall environment E .

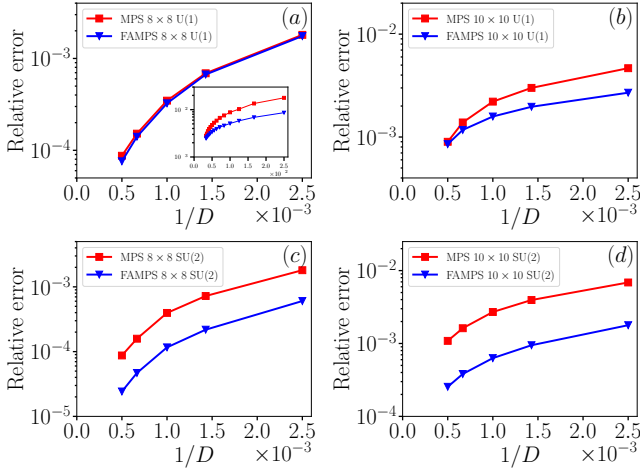


FIG. 2: Relative error of the ground state energy for FAMPS and MPS of the Heisenberg model for lattice sizes 8×8 and 10×10 with open boundary conditions. Simulations in (a) and (b) utilize U(1) symmetry and have a physical bond dimension $d = 2$, while in (c) and (d), we use SU(2) symmetry and have a physical bond dimension $d = 4$ by blocking two sites into one site. We can find that by allowing more free parameters in the disentanglers (in (c) and (d)), the critical bond dimension problem (in (a) and (b)) is solved.

- (ii) perform a Singular Value Decomposition (SVD) for environment $E = USV^\dagger$, then calculate the optimized disentangler $u_{\text{new}} = -VU^\dagger$.
- (iii) move to another disentangler and repeat (i) and (ii) until all the disentanglers are optimized once.

After optimizing the disentanglers for 3 ~ 5 sweeps, we move to the optimization of MPS tensors. The optimization of MPS tensors follows the below steps.

- (i) choose an MPS tensor T , set the tensor T as the center tensor as in MPS optimization algorithm.
- (ii) calculate the environments for this tensor T from all the Hamiltonian terms and add them up to get the overall environment.
- (iii) use the Lanczos or similar algorithm to solve the eigenvalue problem for tensor T . In this step, step (ii) needs to be repeated for several times.
- (iv) move to a next MPS tensor and repeat step (i), (ii) and (iii) until all the MPS tensors are optimized.

Then, we repeat the process by optimizing disentanglers and MPS tensors alternatively until the energy is converged.

Critical Bond Dimension in FAMPS

As mentioned in the main text, in the study of Heisenberg model with open boundary conditions we encounter

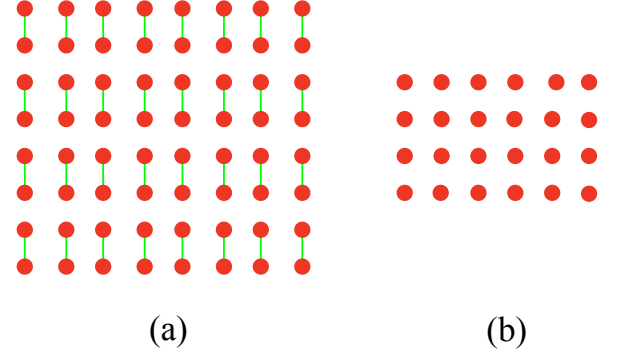


FIG. 3: To increase the number of free parameters in disentanglers for the Heisenberg model, we block two sites linked by green lines in (a) into one site.

the problem of critical bond dimension in FAMPS. The results are shown in Fig. 2. In (a) and (b), we can find that with the increase of bond dimension, there exist a critical bond dimension after which the results of FAMPS and MPS are identical. This phenomenon is related to the absence of free parameters of disentanglers. For spin $1/2$ degree of freedom, each site has physical dimension $d = 2$ and can be labeled by quantum number $\{0, 1\}$. Under U(1) symmetry, disentangler u_{ij}^{kl} can be written as (we only consider real entries for u_{ij}^{kl})

$$u_{ij}^{kl} = u_0 \oplus u_1 \oplus u_2 \quad (7)$$

where u_1 is a 2×2 matrix and u_0, u_2 are 1×1 matrices or numbers. Due to the unitary property of disentangler, $u_0^2 = 1, u_2^2 = 1, u_1^\dagger u_1 = I_{2 \times 2}$. Thus, disentangler u_{ij}^{kl} can be written as

$$u_{ij}^{kl} = \pm 1 \begin{pmatrix} 1 & 0 & 0 & 0 \\ 0 & \sin \theta & \cos \theta & 0 \\ 0 & -\cos \theta & \sin \theta & 0 \\ 0 & 0 & 0 & 1 \end{pmatrix} \quad (8)$$

Thus, disentangler u_{ij}^{kl} has only one free parameter under U(1) symmetry. But under SU(2) symmetry, disentangler u_{ij}^{kl} is written as (using the notation in Ref. [3])

$$u_{ij}^{kl} = (P_0 \otimes Q_{\frac{1}{2}, \frac{1}{2} \rightarrow \frac{1}{2}, \frac{1}{2}}^0) + (P_1 \otimes Q_{\frac{1}{2}, \frac{1}{2} \rightarrow \frac{1}{2}, \frac{1}{2}}^1) \quad (9)$$

where P_0, P_1 are numbers, $Q_{\frac{1}{2}, \frac{1}{2} \rightarrow \frac{1}{2}, \frac{1}{2}}^0$ and $Q_{\frac{1}{2}, \frac{1}{2} \rightarrow \frac{1}{2}, \frac{1}{2}}^1$ are matrix determined by Clebsch-Gordan coefficients, which are $\begin{pmatrix} 0 & 0 & 0 & 0 \\ 0 & 1/2 & -1/2 & 0 \\ 0 & -1/2 & 1/2 & 0 \\ 0 & 0 & 0 & 0 \end{pmatrix}$ and $\begin{pmatrix} 1 & 0 & 0 & 0 \\ 0 & 1/2 & 1/2 & 0 \\ 0 & 1/2 & 1/2 & 0 \\ 0 & 0 & 0 & 1 \end{pmatrix}$ respectively. Under the restriction of $u^\dagger u = I$, $P_0^2 = P_1^2 = 1$, which leads to $P_0 = \pm 1, P_1 = \pm 1$. Thus, disentangler u_{ij}^{kl} has no free parameter under SU(2) symmetry. When considering Z(2) symmetry (in the transverse Ising

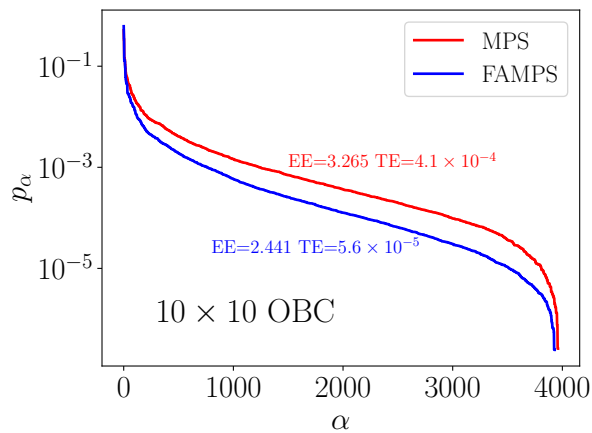


FIG. 4: The distribution of the entanglement spectrum for the Heisenberg model on a 10×10 lattice under open boundary conditions. The bond dimension for both MPS and FAMPS are $D = 1000$. The result for the FAMPS is for the underlying MPS (without disentglers). We can see that both the entanglement entropy (EE) and truncation error (TE) are reduced in FAMPS.

model), disentangler u_{ij}^{kl} can be written as

$$u_{ij}^{kl} = u_0 \oplus u_1 \quad (10)$$

where u_0, u_1 are 2×2 matrix satisfying $u_1^\dagger u_1 = u_2^\dagger u_2 = I_{2 \times 2}$. Then, disentangler u_{ij}^{kl} can be represented as

$$u_{ij}^{kl} = \begin{pmatrix} \sin \alpha & 0 & 0 & \cos \alpha \\ 0 & \sin \beta & \cos \beta & 0 \\ 0 & -\cos \beta & \sin \beta & 0 \\ -\cos \alpha & 0 & 0 & \sin \alpha \end{pmatrix} \quad (11)$$

Here, disentangler u_{ij}^{kl} has two free parameters. Thus, in Transverse Ising model, there is no critical bond dimension as shown in Fig. 2 in the main text.

For the U(1) symmetry imposed DMRG calculations in Fig. 2 (a) and (b), SU(2) symmetry is nearly restored after the critical bond dimension, which means the disentglers have no free parameter and FAMPS results are identical to MPS ones. To solve this problem, we can block two sites into one to enlarge the physical degrees of freedom as shown in Fig. 3. In this way, we increase the number of free parameters in the disentglers. Fig. 2 (c) and (d) show calculations with the same models in Fig. 2 (a) and (b). From Fig. 2, we can find that the FAMPS results are always better than MPS results and there is no critical bond dimension.

Comparison of the entanglement spectrum

In Fig. 4, we show the the distribution of the entan-

glement spectrum for the Heisenberg model on a 10×10

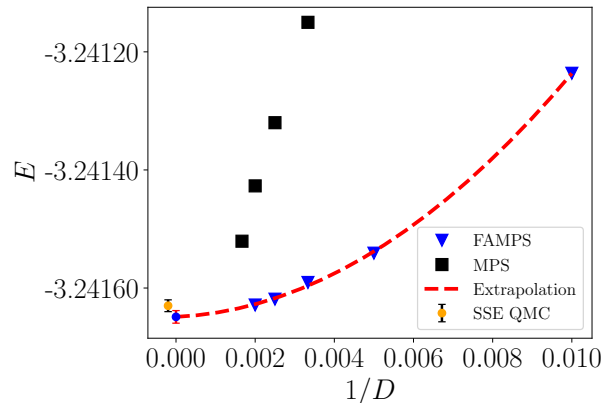


FIG. 5: A quadratic extrapolation of the FAMPS energy per site of a 8×8 transverse Ising model with $\lambda = 3.05$ under periodic boundary conditions. The fit gives an extrapolated value of ground state energy per site $E = -3.24165(1)$ which agrees with the SSE QMC result $-3.24163(1)$ within the error bar.

lattice under open boundary conditions. The bond dimension for both MPS and FAMPS are $D = 1000$. The result for the FAMPS is for the underlying MPS (without disentglers). We can see that both the entanglement entropy (EE) and truncation error (TE) are reduced in FAMPS, which demonstrates the effect of disentglers to reduce the entanglement in the ground state wavefunction and hence to increase the accuracy of MPS.

More Results

In Fig. 5, we show the extrapolation of FAMPS energy with bond dimension for the transverse Ising model with periodic boundary conditions and $\lambda = 3.05$ on a 8×8 lattice. A quadratic fit gives the extrapolated value of ground state energy per site $E = -3.24165(1)$ which agrees with the SSE QMC result $-3.24163(1)$ within the error bar.

* qinmingpu@sjtu.edu.cn

- [1] G. Evenbly and G. Vidal, Phys. Rev. B **79**, 144108 (2009), URL <https://link.aps.org/doi/10.1103/PhysRevB.79.144108>.
- [2] T. Felser, S. Notarnicola, and S. Montangero, Phys. Rev. Lett. **126**, 170603 (2021), URL <https://link.aps.org/doi/10.1103/PhysRevLett.126.170603>.
- [3] S. Singh and G. Vidal, Phys. Rev. B **86**, 195114 (2012), URL <https://link.aps.org/doi/10.1103/PhysRevB.86.195114>.